scientific reports

Check for updates

OPEN

Electromagnetic waves destabilize the SARS-CoV-2 Spike protein and reduce SARS-CoV-2 Virus-Like particle (SC2-VLP) infectivity

Christina Pantoja[1,3], Francisco M. Acosta[1,3], Skyler Granatir[2,3], Michael Anderson[1], Maya Wyr[1], Johann Tailor[1], Angus Fuori[1], William Dower[2], H. Bo Marr[2] & Peter W. Ramirez[1]✉

Infection and transmission of Severe Acute Respiratory Syndrome Coronavirus 2 (SARS-CoV-2) continues to pose a global public health concern. Using electromagnetic waves represents an alternative strategy to inactivate pathogenic viruses such as SARS-CoV-2. However, whether electromagnetic waves reduce SARS-CoV-2 infectivity is unclear. Here, we adapted a coplanar waveguide (CPW) to identify frequencies that could potentially neutralize SARS-CoV-2 virus-like particles (SC2-VLPs). Treatment of SC2-VLPs at frequencies between 2.5 and 3.5 GHz and an electric field of 413 V/m reduced infectivity. Exposure of SC2-VLPs to a frequency of 3.1 GHz –and to a lesser extent, 5.9 GHz– reduced their binding to antibodies targeting the SARS-CoV-2 Spike S1 receptor-binding domain (RBD) but did not alter the total levels of Spike, Nucleocapsid, Envelope, or Membrane proteins in virus particles. These results suggest that electromagnetic waves alter the conformation of Spike, thereby reducing viral attachment and entry. Overall, this data provides proof-of-concept in using electromagnetic waves for sanitation and prevention efforts to curb the transmission of SARS-CoV-2 and potentially other pathogenic enveloped viruses.

Keywords SARS-CoV-2, Spike, Electromagnetic waves, Coplanar waveguide, Transmission, Sanitation

Coronaviruses consist of a family of enveloped positive-sense single-stranded RNA (+ ssRNA) viruses that infect a wide variety of mammals and can cause mild or severe disease[1]. Three human coronaviruses emerged in the 21st century that pose a significant threat to public health: severe acute respiratory syndrome coronavirus 1 (SARS or SARS-CoV-1), middle east respiratory syndrome (MERS) and severe acute respiratory syndrome coronavirus 2 (SARS-CoV-2)[2–5]. SARS-CoV-2 is the causative agent of the COVID-19 pandemic[6]. Viral transmission of human coronaviruses occurs via person-to-person contact, respiratory droplets, and through touching contaminated surfaces[7]. As of April 2025, SARS-CoV-2 has infected nearly 800 million individuals and led to over 7 million deaths (WHO). Despite effective vaccines[8] and therapeutics[9,10], SARS-CoV-2 continues to circulate and can lead to complications, particularly in high-risk groups. Therefore, increased strategies to curb SARS-CoV-2 transmission are needed.

Standard pathogen disinfection includes the use of high temperatures, ultraviolet and ionizing radiation, and chemical agents, though these techniques have limitations[11–15]. Electromagnetic waves offer an alternative strategy to inactivate viruses, possessing high penetration, uniform heating, and minimal pollution[16]. How electromagnetic waves alter virus infectivity is an active area of investigation, though it can include changes in virus morphology[15,17], damage to viral RNA[18] and denaturation of enveloped virus glycoproteins[19].

The SARS-CoV-2 Spike glycoprotein mediates attachment and entry into host cells. Spike contains S1 and S2 subunits that exist in a glycosylated trimeric form on the surface of a mature virus. The S1 receptor binding domain (RBD) facilitates binding to host angiotensin converting enzyme 2 (ACE2)[5]. A polybasic cleavage site (RRAR) is present at the junction between the S1 and S2 subunits, which is cleaved by the host protease furin during virus assembly to expose an S2' site[20]. Cleavage of the S2' site by the host serine protease TMPRSS2 exposes a fusion peptide (FP), which inserts into the host cell membrane to mediate viral fusion and entry at the cell surface[20,21]. In cells lacking TMPRSS2 or if ACE2/virus complexes fail to interact with TMPRSS2,

[1]Department of Biological Sciences, California State University Long Beach, Long Beach, CA, USA. [2]Epirus Inc., Torrance, CA, USA. [3]Christina Pantoja, Francisco M. Acosta and Skyler Granatir: These authors contributed equally to this work. ✉email: Peter.Ramirez@csulb.edu

SARS-CoV-2 entry occurs via clathrin-mediated endocytosis, with Spike cleavage occurring in a pH-dependent manner mediated by the cysteine protease cathepsin L[22].

The goal of this study was to determine whether electromagnetic waves could affect the infectivity of SARS-CoV-2. For our studies, we adapted a system using SARS-CoV-2 virus-like particles (SC2-VLPs) that package and deliver exogenous RNA transcripts (i.e. luciferase) into target cells[23]. Because SC2-VLPs contain each of the SARS-CoV-2 structural proteins (Spike, Nucleocapsid, Envelope and Membrane), they recapitulate authentic aspects of SARS-CoV-2 entry, assembly and release and are suitable to work with in a Biosafety Level 2 (BSL2) setting. We employed a coplanar waveguide (CPW) to determine the absorption spectrum of SC2-VLPs. We then tested a range of electromagnetic wave frequencies to determine whether they had any effect on reducing SC2-VLP infectivity. We found that frequencies within 2.5–3.5 GHz reduced infectivity when exposing SC2-VLPs to an electric field of 413 V/m. This correlated with reduced binding of SC2-VLPs to antibodies specific for the Spike S1 RBD but did not alter the total protein levels of Spike, Nucleocapsid, Envelope nor Membrane in virus particles. This suggests that electromagnetic waves induce conformational changes within Spike that negatively impact viral attachment/entry into host cells. To our knowledge, this is the first study to provide direct experimental evidence that electromagnetic waves can reduce SARS-CoV-2 infectivity, along with a plausible mechanism underlying this effect. These findings offer a promising proof-of-concept for the potential use of electromagnetic waves to mitigate COVID-19 transmission.

Results

Identification of electromagnetic waves absorbed by SC2-VLPs using a coplanar waveguide (CPW)

To generate electromagnetic waves, we created a setup consisting of a computer, function and signal generators, oscilloscope, amplifier, and transverse electromagnetic (TEM) cell (Fig. 1). Electromagnetic waves originated from the signal and function generator, while a computer connected to all equipment set parameters such as pulse width, input power, and frequency. Once triggered by the function generator, the signal generator transmitted waveforms to a wideband amplifier, outputting a 180–250 W signal to the TEM cell through N-connector cables.

We used a coplanar waveguide (CPW) in combination with a Vector Network Analyzer (VNA) to identify electromagnetic waves absorbed by SC2-VLPs. We modeled our design after Yang et al., who designed a CPW circuit to measure the electromagnetic wave absorption spectra of H3N2 influenza viruses[24]. A CPW is a waveguide in which all conductors supporting wave propagation are placed on the same plane. Active

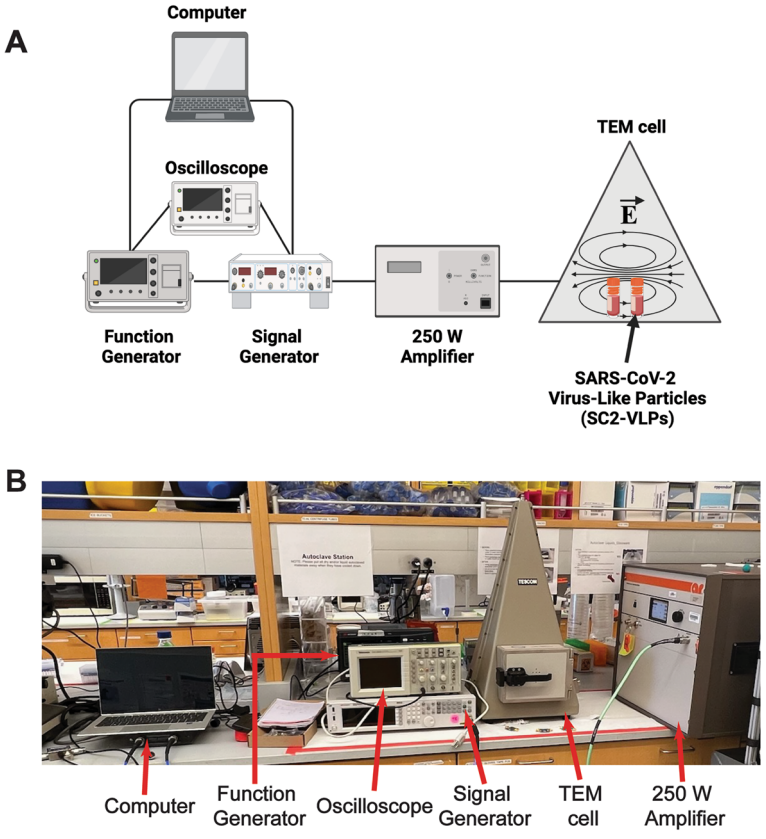

Fig. 1. Electromagnetic wave hardware setup. **(A)** Graphical diagram. A computer-controlled function and signal generator produced electromagnetic waves, which were sent to an amplifier and delivered to a TEM cell through N-connector cables. The TEM served as a unit to conduct electromagnetic wave testing, while an oscilloscope was used to detect electrical signals. **(B)** Image of setup. TEM: transverse electromagnetic cell.

components can be placed along a microstrip (Fig. 2A). Each end of the CPW is connected to a VNA, which can emit and receive thousands of frequency points over a short interval of time (Fig. 2B). In this manner, the absorption of any fluid along the microstrip can be determined. A higher absorption implies a greater electromagnetic wave permittivity at a given frequency. This can lead to changes in virus architecture, rendering them non-infectious. To obtain an absorption spectrum for SC2-VLPs, we dripped them uniformly along our CPW microstrip (Fig. 2A) and observed local peaks around 3.1 GHz and 6 GHz (Fig. 2C).

Electromagnetic waves reduce SARS-CoV-2 virus like particle (SC2-VLP) infectivity

Next, we determined whether exposing SC2-VLPs to electromagnetic waves could affect their infectivity. To do this, mammalian expression plasmids encoding Spike, Nucleocapsid, Envelope, Membrane and a transfer plasmid (Luc-PS9) were transfected into HEK293T cells. SARS-CoV-2 structural proteins formed virus-like particles (SC2-VLPs), while the transfer plasmid encoded a luciferase transcript and packaging signal (PS9) that enabled Nucleocapsid to recognize, package, and deliver exogenous transcripts[23]. Luciferase activity was measured by incubating SC2-VLPs with HEK293T cells expressing ACE and TMPRSS2 (Fig. 3A). After producing SC2-VLPs, we verified that Spike, Nucleocapsid, Envelope, and Membrane were expressed (Fig. 3B; Supplementary Fig. 1). We then exposed SC2-VLPs to a range of frequencies (1–6 GHz) based on our absorption spectra (Fig. 2C), at a power density of 413 V/m and radiation times varying from 2 to 10 min. As a control, we exposed SC2-VLPs to 2.45 GHz microwave (MW) radiation, which has been shown to inactivate Hepatitis C Virus (HCV) and Human Immunodeficiency Virus (HIV-1), as well as denature the SARS-CoV-2 Spike protein in vitro[19,25]. We compiled our data into the following frequency ranges: Unexposed, 1.0–2.5 GHz, 2.5–3.5 GHz, 3.5–4.8 GHz, 4.8–6 GHz, and MW. Unexposed referred to samples placed in the TEM cell for a set time without electromagnetic wave exposure. Overall, SC2-VLP infectivity decreased with exposure to either electromagnetic waves or MW radiation. However, the strongest reduction in infectivity occurred when SC2-VLPs were exposed to 2.5–3.5 GHz electromagnetic waves (Fig. 3C), aligning with our absorption spectra (Fig. 2C).

Electromagnetic waves destabilize the SARS-CoV-2 Spike receptor binding domain (RBD)

We next sought to determine the mechanism by which electromagnetic waves reduced the infectivity of SC2-VLPs. Two potential hypotheses emerged, one being that electromagnetic waves alter the conformation of the Spike protein, reducing its ability to bind to ACE2[19,26], and the other proposing that electromagnetic waves may be physically destroying our SC2-VLPs[12,24,27]. To test these, we exposed SC2-VLPs to frequencies (3.1 GHz; 5.9 GHz) that exhibited the highest levels of absorption (Fig. 2C) and/or reduced infectivity (Fig. 3C). We then measured the ability of untreated or treated SC2-VLPs to (1) bind an antibody targeting the Spike S1 receptor binding domain (S1RBD) via Enzyme-Linked Immunosorbent Assay (ELISA) or (2) isolated virus particles and probed for SARS-CoV-2 structural proteins by Western blot (Fig. 4A). Interestingly, SC2-VLPs treated with

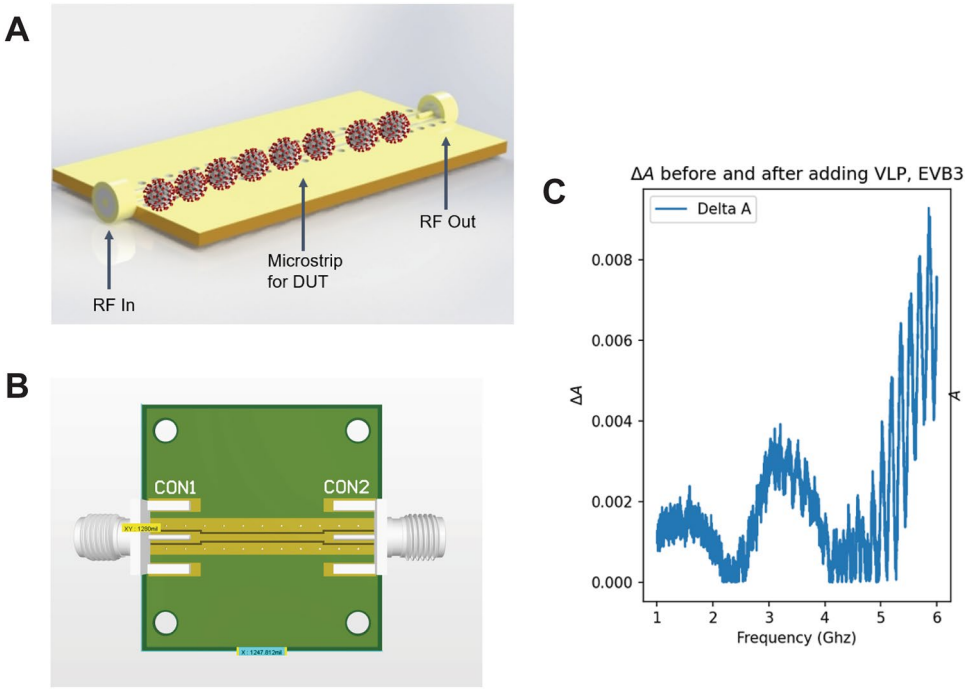

Fig. 2. Coplanar Waveguide (CPW) setup and absorption spectra of SARS-CoV-2 Virus-Like Particles (SC2-VLPs). **(A)** Illustration of a virus solvent suspended on a CPW. **(B)** Epirus CPW circuit. **(C)** SC2-VLP absorption spectra. ΔA reflects the amount of radiation absorbed by SC2-VLPs. RF: Radio-Frequency signal. DUT: Device-Under-Test.

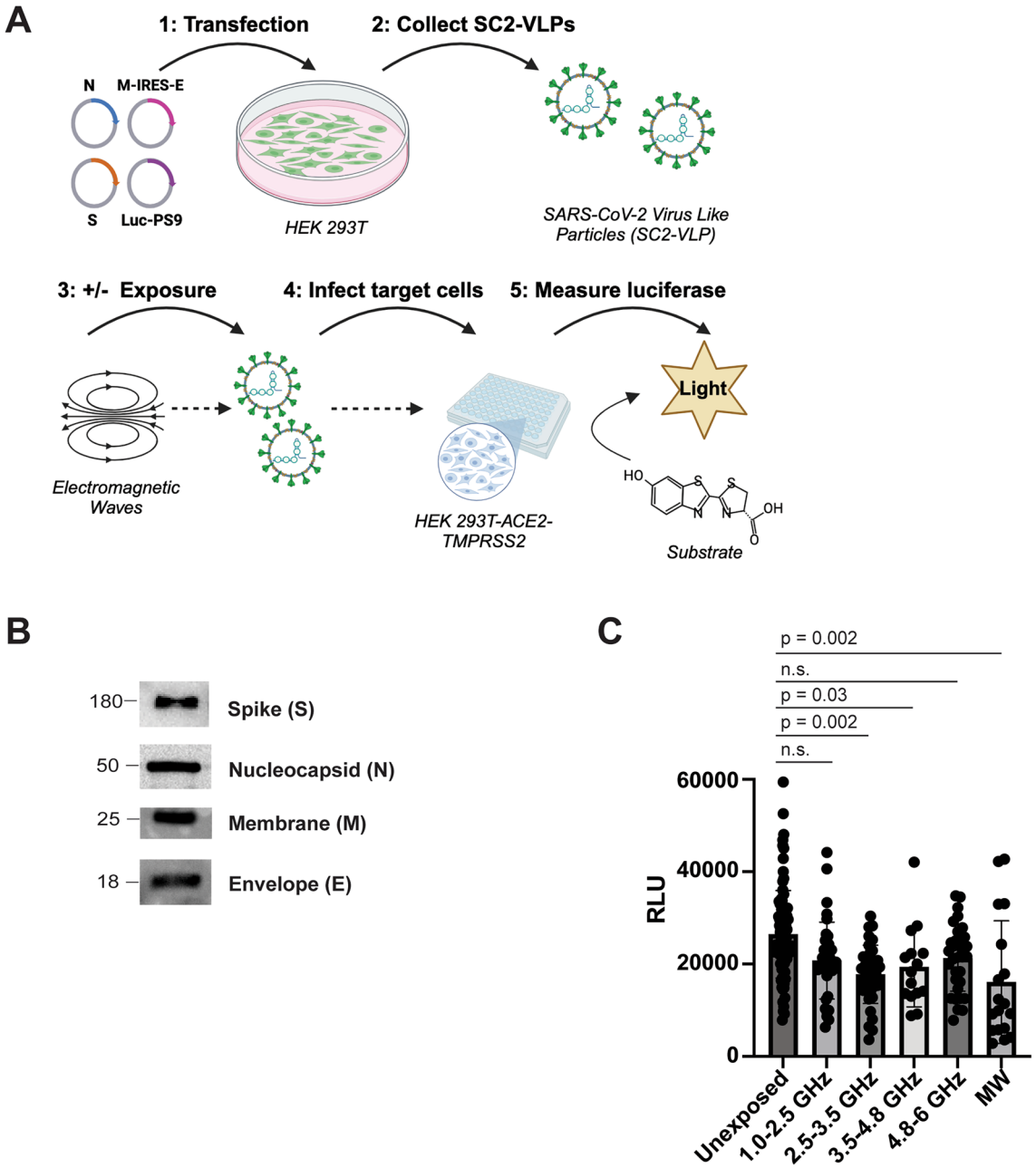

Fig. 3. Electromagnetic waves reduce infectivity of SARS-CoV-2 Virus-Like Particles (SC2-VLPs). **(A)** Diagram of SC2-VLP production, electromagnetic wave treatment and infectivity assay. Plasmids expressing each of the SARS-CoV-2 structural proteins (Nucleocapsid (N); Matrix (M); Envelope (E); and Spike (S)), or a plasmid encoding a packaging signal and luciferase transcript (Luc-PS9) were transfected into viral producer cells (HEK293T). SC2-VLPs were then collected, left unexposed or exposed to various electromagnetic wave frequencies (1–6 GHz) and used to infect target cells (HEK293T-ACE2-TMPRSS2). The next day, luciferase was measured as a readout of infectivity. Created in https://BioRender.com. **(B)** Western blot of pelleted Spike (S), Nucleocapsid (N), Membrane (M), Envelope (E) in unexposed virus particles. The image is representative of two independent experiments. **(C)** SC2-VLP infectivity assay. Frequencies (1–6 GHz) were tested over a range of exposure times (2–10 min). Data represent compiled mean +/- SD of 5 independent experiments. The luciferase signal for each frequency/exposure time was performed in triplicate. P-values indicate Wilcoxon matched-pair signed rank test of unexposed compared to exposed samples. ($n = 90$ (Unexposed); $n = 36$ (1.0–2.5 GHz & 2.5–3.5 GHz) $n = 15$ (3.5–4.8 GHz), $n = 33$ (4.8–6 GHz), $n = 18$ (MW)). RLU: Renilla Luciferase Units (RLU). MW: Microwave.

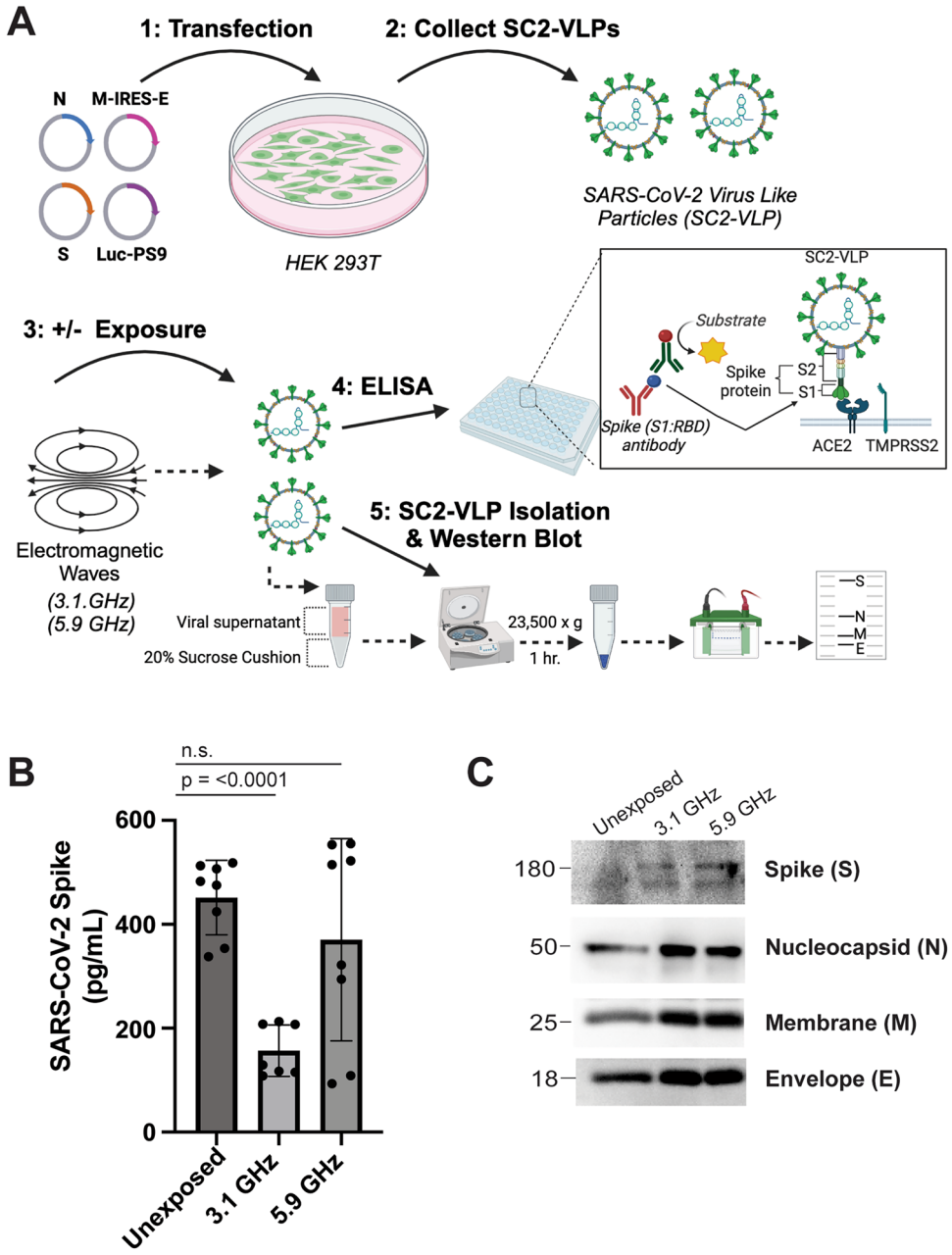

Fig. 4. Electromagnetic waves destabilize SARS-CoV-2 Spike. **(A)** SC2-VLPs were produced, collected, and either unexposed or exposed to 3.1 or 5.9 GHz electromagnetic waves for 8 min. SC2-VLPs were either subjected to an ELISA to measure binding to antibodies targeting the Spike Subunit 1 receptor-binding domain (S1RBD) or pelleted and probed for Spike (S), Nucleocapsid (N), Membrane (M), and Envelope (E) by western blot. Created in https://BioRender.com. **(B)** Spike (S1RBD) ELISA. Data represent +/- SD of 2 independent experiments performed in quadruplicate, except for one condition (3.1 GHz) that was analyzed once in quadruplicate and once in triplicate. P-values indicate one-way ANOVA tests of treated compared to untreated samples. **(C)** Western blot depicting Spike (S), Nucleocapsid (N), Membrane (M), and Envelope (E) within pelleted virus particles. The image is representative of two independent experiments.

3.1 GHz, and to a lesser extent 5.9 GHz, bound less efficiently to an S1RBD-specific antibody by approximately 70% and 15% (Fig. 4B). In contrast, we detected no overt differences in the expression of Spike, Nucleocapsid, Envelope, nor Membrane proteins in SC2-VLPs exposed to 3.1–5.9 GHz (Fig. 4C; Supplementary Fig. 2). The weak Spike expression in our unexposed SC2-VLP sample likely occurred due to transfer issues, since a robust Spike signal was detected in our ELISA assay (Fig. 4B). Overall, these data support a model whereby electric fields alter the conformation of Spike, negatively impacting its ability to bind ACE2 to enter cells.

Discussion

This study sought to determine the role of using electromagnetic waves to inactivate enveloped viruses, particularly SARS-CoV-2. We present the first proof-of-concept study showing that nonthermal electromagnetic waves of 2.5–3.5 GHz at 413 V/m alter the conformation of the SARS-CoV-2 Spike S1 RBD, reducing the infectivity of SC2-VLPs.

Mechanistically, inactivation of viruses using electromagnetic waves can occur due to thermal, nonthermal, or physical resonance effects. Thermal effects inactivate viruses by increasing the surrounding temperature. Exposing human coronavirus 229E to electromagnetic waves of 95 GHz at a power density of 70–100 W/cm^2 for 2 seconds led to virus inactivation induced by a 100° C change in temperature[15]. This resulted in drastic changes to virus morphology, forming holes in the envelope of 229E virions revealed by scanning electron microscopy (SEM)[15]. Siddharta et al. significantly reduced or completely inactivated Human Immunodeficiency Virus (HIV-1) and diverse Hepatitis C Virus (HCV) genotypes using microwave irradiation at power densities between 360 W – 800 W[25]. All HCV genotypes required a temperature of 56–60 °C to reduce infectivity by 90%, a threshold attainable using 360 W of power for 2 minutes[25]. A recent study reported a 9.375 GHz frequency at 100 mW/cm^2 inactivated coronavirus mouse hepatitis A59 (MHV-A59) by physical destruction of the viral envelope and genome[27]. However, whether these phenomena occurred due to changes in thermal or physical resonance effects were not explored. Here, we did not detect any changes in temperature when subjecting SC2-VLPs to various electromagnetic frequencies (data not shown), suggesting our results occurred in a nonthermal manner.

Physical resonance effects occur when objects absorb more energy from their surrounding environment when vibrating at their natural frequency and wavelength. Viruses resonate in the confined-acoustic dipolar mode with electromagnetic waves of the same frequency[16,24]. This leads to a structure resonance energy transfer (SRET) from electromagnetic waves to confined acoustic vibrations (CAV) in viruses, inducing fracture of the virus structure. Indeed, inactivation of influenza A virus strain H3N2 occurred when exposing the virus to a frequency of 6 GHz at 486 W/m^2 power density, resulting in the physical rupture of the viral envelope through resonance effects despite minimal increases in temperature[24]. Another study reported a 3-log reduction in viral infectivity with Human Coronavirus 229E, attributed to non-thermal structural damage induced via the SRET effect[28]. Notably, exposure of SC2-VLPs to electromagnetic waves that reduced infectivity did not decrease protein levels of Spike, Nucleocapsid, Envelope or Membrane (Fig. 4C). These findings do not support a physical resonance model that destroys virus particles and/or viral proteins. However, we cannot entirely rule out the possibility that the frequencies used in our study did not physically rupture virus particles. Future studies should seek to address this using electron microscopy.

Electromagnetic waves can cause molecules to rotate or vibrate in a nonthermal manner, altering their polarity to induce changes in the conformation of viral proteins. Irradiating SARS-CoV-2 Spike with non-thermal microwave radiation (700 W 2.45 GHz) denatured the S1 subunit by 95% in experiments conducted in vitro[19]. Thus, conformational changes in Spike occurred due to pure electromagnetic effects. Another study used molecular simulations to conclude that exposure to electric fields can alter the conformation of SARS-CoV-2 Spike and its variants, negatively impacting its ability to bind to ACE2[26]. Specifically, applying electric fields induced a conformational change in the recognition loop L3 of the Spike RBD, converting two parallel b-sheets into an unstructured coil, thereby reducing ACE2 binding[26]. Interestingly, follow-up simulations reported minimal structural damage to the Spike S2 subunit, suggesting Spike's susceptibility to electric fields is limited to its prefusion (S1 subunit), rather than post fusion (S2 subunit) conformational state[29]. Although preliminary, our data provide experimental support for a nonthermal mechanism: exposure of SC2-VLPs to 3.1 and 5.9 GHz electromagnetic waves reduced Spike binding to antibodies targeting the S1 RBD (Fig. 4B). Notably, the SARS-CoV-2 Spike protein engages not only ACE2 but also several other cellular proteins and molecules via its RBD to facilitate viral entry[30]. This includes Asialoglycoprotein receptor 1 (ASGR1), CD147, CD4, Heparan Sulfate, Kringle containing transmembrane protein 1 (KREMEN1), Lectins, Niemann-Pick C1 (NPC1), Sialic Acids, TMEM10B and Transferrin Receptor (TfR)[30–39]. Thus, electromagnetic wave-induced conformational changes in Spike may impair the virus's capacity to exploit alternative entry pathways, potentially restricting viral tropism, especially in cells with low or absent ACE2 expression. Nonetheless, further investigation is required to substantiate our findings. For instance, future studies could evaluate how electromagnetic wave exposure affects Spike's binding to ACE2 or alternate receptors by using peptidomimetics or glycomimetic compounds. In addition, circular dichroism (CD) spectroscopy could be employed to detect potential changes in Spike's secondary structure post-exposure to electromagnetic waves. Finally, it would be of interest to determine whether the S2 subunit of Spike, in contrast to S1, exhibits relative resistance to electromagnetic waves.

Our study has limitations. First, SC2-VLPs may not wholly reflect what occurs in cells infected with SARS-CoV-2. Because SARS-CoV-2 is classified as a BSL3 agent, we did not have the research facilities to perform work with this pathogen. However, because SC2-VLPs mimic the viral assembly, packaging, production, and delivery of exogenous transcripts, they provide important insights into the mechanisms governing SARS-CoV-2 replication, including attachment and entry. Nonetheless, future studies should address whether electromagnetic fields can reduce the infectivity of authentic replication-competent SARS-CoV-2. Second, due to budgetary and equipment constraints, we were unable to determine whether SARS-CoV-2 variants are susceptible to electromagnetic fields. Here, we created SC2-VLPs using a plasmid expressing the SARS-CoV-2 Spike protein derived from the original Wuhan-1 strain[23]. Exposure to electric fields via molecular simulations induced structural changes within the SARS-CoV-2 Spike RBDs from wildtype (Wuhan-1) as well as Alpha (B.1.1.7), Beta (B.1.351), Gamma (P.1), Delta (B.1.617.2), and Omicron (BA.1) variants[26,29]. We hypothesize that the structural damage induced by electric fields towards ancestral Spike will extend to other Spike variants. However, this has yet to be experimentally tested. Finally, whether our CPW/VNA system reduces the infectivity of IAV, HIV-1, HCV or other pathogenic enveloped viruses is intriguing but was beyond the scope of this study.

What are the advantages of using electromagnetic waves for virus inactivation over other disinfection methods, such as ultraviolet (UV-C) light? Numerous studies have reported that UV-C (254 nm) and far UV-C (222 nm) can inactivate SARS-CoV-2[40–43]. While this approach is widely applicable, it does have limitations. First, while UV-C primarily disinfects surfaces, electromagnetic waves can penetrate a wider variety of materials. For example, a 9.375 GHz electromagnetic wave significantly reduced the infectivity of the coronavirus MHV-A59 on diverse surfaces, including plastic, glass, cloth, and wood[27]. This penetrative capability expands the opportunities to employ electromagnetic waves for clinical applications. Portable electromagnetic wave-based sterilization units could be used in hospitals to disinfect beds, monitors, and other heat- or moisture-sensitive equipment. Such approaches may complement existing protocols to enhance infection control in high-risk healthcare environments. Second, UV-C primarily inactivates viruses by damaging their genetic material, whereas electromagnetic waves can disrupt molecular bonds beyond DNA and RNA. This study and others showed that the SARS-CoV-2 Spike protein is vulnerable to electric fields, presumably leading to changes in its conformation that negatively impact receptor binding[19,26]. Third, UV-C lamps produce harmful byproducts like ozone and/or mercury[44], whereas electromagnetic waves do not. Fourth, electromagnetic waves may be more cost-effective and scalable. UV-C and far UV- lamps require frequent replacement and consume energy, making long-term maintenance expensive. In contrast, electromagnetic wave-based sterilization could be easily integrated into existing infrastructure — such as HVAC units — to continuously inactivate airborne viruses, especially in research laboratories and hospital wards. Finally, electromagnetic waves may offer a safer alternative to UV-C for virus inactivation. Extended exposure to UV-C can cause skin/eye irritation, increase the risk of cancer, and accelerate premature aging[45]. Far UV-C is safer, though exposure limits and ozone production still exist[46]. Alternatively, FDA-approved pulsed electromagnetic field (PEMF) therapy is currently being used and/or studied for the treatment of several conditions including trauma (i.e. bone fractures) and musculoskeletal disorders[47,48]. PEMF is a non-invasive treatment that applies low frequency, pulsed electromagnetic fields to targeted areas of the body. These pulses penetrate tissue, enhancing cellular ion exchange, mitochondrial function, and blood circulation, thereby stimulating cellular activity, and accelerating wound healing[48]. Although PEMF therapy shows promise, further research is needed to determine whether the electromagnetic wave frequencies that inactivate viruses are also safe for human cells and tissues. Collectively, perhaps combining UV-C and electromagnetic wave technology may provide the most effective solution for virus inactivation.

In summary, electromagnetic waves offer an intriguing strategy to inactivate pathogenic viruses. By using a unique CPW and VNA, we rapidly obtained the absorption spectrum of SC2-VLPs, providing insightful information about the permittivity and susceptibility of SARS-CoV-2 to certain electromagnetic wave frequencies. Identifying electromagnetic waves that have minimal impacts on the human body may offer novel in-vivo methods for neutralizing pathogenic viruses. Beyond inactivation, the CPW technique employed here could potentially be used to detect viruses with a priori knowledge of the virus's absorption characteristics. Deployment of a portable system utilizing a VNA-like circuit could measure absorption at the most informative frequencies in a wide range of samples. Thus, electromagnetic waves provide several encouraging future developments to improve viral detection, inactivation, and sanitation.

Materials and methods

Cell Lines and Plasmids

HEK293T (ATCC; CRL-3216) were maintained in complete DMEM (Thermo Fisher Scientific): 10% fetal bovine serum (FBS; Corning), glutamine (Thermo Fisher Scientific) and 1% penicillin/streptomycin (Thermo Fisher Scientific). HEK293 cells expressing human ACE2 and TMPRSS2 (Invivogen; hkb-hace2 tpsa) were propagated in complete DMEM supplemented with puromycin (0.5 mg/ml), hygromycin B (200 mg/ml) and zeocin (100 mg/ml). The following plasmids were gifts from Dr. Jennifer Doudna and purchased from Addgene: CoV-2-N-WT-Hu1 (#177937), CoV-2-M-IRES-E (#177938), CoV-2-Spike-EF1a-D614G-N501Y (#177939), and Luc-PS9 (#177942).

Generation of SARS-CoV-2 Virus-Like particles (SC2-VLPs)

HEK293T cells (3.5×10^6 in 10 mL total volume) were seeded in 10 cm dishes 24 h prior to transfection. The next day, cells were transfected with a total of 20 µg plasmid DNA according to the following molar ratios: *1* CoV2-N-WT-Hu1, *0.5* CoV-2-M-IRES-E, *0.5* Luc-PS9 and *0.0125* CoV2-Spike-EF1a-D614G-N501Y. Plasmids were diluted in water to a final volume of 400 µL, along with 100 µL 2.5 M calcium chloride ($CaCl_2$) and 500 µL 2X Hepes Buffered Saline (HBS; pH 7.05). This transfection mixture was vortexed, incubated for 1 min at room temperature and added dropwise over the entire culture dish. To increase transfection efficiency, 10 µL of chloroquine (100 mM; Invivogen) was added prior to returning cells to the incubator (37 °C; 5% CO_2). Media was changed 16–18 h post transfection. Forty-eight hours post transfection, supernatant (SC2-VLPs) was collected, clarified by centrifugation, filtered (0.45 µM PES), and stored at −80 ˚C.

Electromagnetic wave generation and exposure

The hardware setup consisted of a computer, function generator (Keysight EDU33212A), signal generator (Keysight MXG N5182B) oscilloscope (Tektronic TDS2001C), amplifier (AR Worldwide 250 A250A), and transverse electromagnetic cell (TEM; Tescom TC-5062C). The TEM cell possessed a shielded enclosure that provided powerful electric fields (200–2000 V/m). An input power of 180 W, corresponding to 413 V/m was used for all experiments. Any leaked radiation was below 5 mV/cm^2, the FCC human safety threshold. For electromagnetic wave exposure, 1.5 ml polypropylene microcentrifuge tubes (Fisher Scientific) containing SC2-VLPs in solution (DMEM media) were placed in the middle of the TEM cell. For infectivity experiments, SC2-VLPs were subjected to frequencies between 1 and 6 GHz and exposure times ranging from 2 to 10 min. For ELISA and western blot experiments (Fig. 4), SC2-VLPs were exposed to 3.1 and 5.9 GHz frequencies for

8 min. Control "Unexposed" SC2-VLPs were placed in the TEM cell and subjected to the same conditions as the exposed SC2-VLPs, but without electromagnetic radiation.

SC2-VLP infection and luciferase readout

In a clear, sterile, 96-well round-bottom plate, 30,000 HEK293T/ACE2/TMPRSS2 cells were plated per well and either left uninfected or incubated with 50 µL SC2-VLPs in triplicate. Cells and SC-VLPs were incubated (37 °C; 5% CO_2) overnight. The next day, supernatant was removed, cells rinsed with 100 µL 1X PBS (ThermoFisher) and lysed with 20 µL passive lysis buffer (Promega) for 15 min at room temperature with gentle rocking. The cells were then transferred to an opaque white 96-well flat-bottom plate, mixed with 50 µL reconstituted luciferase assay buffer (Promega), and luciferase measured immediately on a plate reader (Biotek Synergy H1). The data was expressed as Relative Light Units (RLU).

Enzyme-linked immunosorbent assay (ELISA)

All reagents, standards, and samples were prepared according to the manufacturer's instructions (RayBiotech; Catalog #: ELV-COVID19S1). Briefly, 100 uL of diluted standard or sample (unexposed or exposed SC2-VLPs) was added to a 96-well plate in duplicate and incubated for 2.5 h. After incubation, wells were washed and incubated with 100 uL of 1X biotinylated antibody for 1 h. Following washing, wells were incubated with 100 uL of 1X streptavidin solution for 45 min. After a final wash step, 100 uL of a TMB One-Step substrate reagent was added to each well for 30 min in the dark, followed by the addition of 50 uL Stop Solution. Absorbance was read immediately at 450 nm on a plate reader (Biotek Synergy H1). All incubation steps were carried out at room temperature.

Virion isolation

SC2-VLPs either unexposed or exposed to electromagnetic waves were overlayed over a 20% sucrose/1XPBS cushion in 2 ml screwcap tubes (Fisher Scientific). Samples were centrifuged (Beckman Coulter Allegra X-30R; F2402H Rotor) at 23, 500 x g for 1 h at 4 °C. Liquid was aspirated, and the virus pellet resuspended in equal volumes of NP-40 lysis buffer (Fisher Scientific) and 2X Laemmli buffer (Bio-Rad).

Western blots

Pelleted SARS-CoV-2 Virus-Like Particles were boiled at 95 °C for 10 min prior to loading onto 12% SDS-PAGE gels. Virions were transferred to a polyvinylidene difluoride (PVDF) membrane (Thermo Fisher Scientific) using the Trans-Blot Turbo System (Bio-Rad) and blocked for 1 h in blocking buffer (1X PBS-Tween 20 (PBST) + 5% milk) at room temperature. Membranes were then incubated overnight with primary antibodies diluted in buffer (1X PBST + 2% Milk) at 4 °C. The following day, membranes were washed 3 times with 1X PBS-T, probed with secondary antibodies diluted in buffer (1X PBST + 2% Milk) for 2 h at room temperature, and washed an additional three times in 1X PBS-T prior to imaging. Membranes were developed using Clarity Enhanced Chemiluminescent (ECL) Substrate (Bio-Rad) and imaged using the iBright imager (Invitrogen). The following antibodies were used: Mouse anti-SARS-CoV-2 Spike (Genetex; Cat # GTX632604), Rabbit anti-SARS-CoV-2 Nucleocapsid (Genetex; Cat # GTX135357), Rabbit anti-SARS-CoV-2 Envelope (Thermo Fisher; Cat # MA5-47046), Rabbit anti-SARS-CoV-2 Membrane (Thermo Fisher; Cat # MA5-46924), Peroxidase-conjugated AffiniPure Goat anti-mouse IgG (Jackson ImmunoResearch; Cat # 115-035-003), Peroxidase-conjugated AffiniPure Goat anti-rabbit IgG (Jackson ImmunoResearch; Cat # 111-035-003).

Data analysis and statistics

Data were analyzed and compiled in Microsoft Excel and GraphPad Prism software (Version 10). Statistical tests were performed in Graph Prism. Significance between samples was assessed using either a Wilcoxon ranked sum test or Analysis of Variance (ANOVA). P values are denoted on the figures. Figures were produced using Adobe Illustrator (CS5) and BioRender software.

Data availability

All data supporting the findings of this study are available within the manuscript or by request.

Received: 11 September 2024; Accepted: 9 May 2025
Published online: 15 May 2025

References

1. Kung, Y. A. et al. Molecular virology of SARS-CoV-2 and related coronaviruses. *Microbiol. Mol. Biol. Rev.* **86**, e00026–e00021 (2022).
2. Kuiken, T. et al. Newly discovered coronavirus as the primary cause of severe acute respiratory syndrome. *Lancet* **362**, 263–270 (2003).
3. Peiris, J. S. M. et al. Coronavirus as a possible cause of severe acute respiratory syndrome. *Lancet* **361**, 1319–1325 (2003).
4. Zaki, A. M., Van Boheemen, S., Bestebroer, T. M., Osterhaus, A. D. M. E. & Fouchier, R. A. M. Isolation of a novel coronavirus from a man with pneumonia in Saudi Arabia. *N Engl. J. Med.* **367**, 1814–1820 (2012).
5. Zhou, P. et al. A pneumonia outbreak associated with a new coronavirus of probable Bat origin. *Nature* **579**, 270–273 (2020).
6. Zhu, N. et al. A novel coronavirus from patients with pneumonia in China, 2019. *N Engl. J. Med.* **382**, 727–733 (2020).
7. Wang, C. C. et al. Airborne transmission of respiratory viruses. *Science* **373**, eabd9149 (2021).
8. Polack, F. P. et al. Safety and efficacy of the BNT162b2 mRNA Covid-19 vaccine. *N Engl. J. Med.* **383**, 2603–2615 (2020).
9. Owen, D. R. et al. An oral SARS-CoV-2 Mpro inhibitor clinical candidate for the treatment of COVID-19. *Science* **374**, 1586–1593 (2021).
10. Wen, W. et al. Efficacy and safety of three new oral antiviral treatment (molnupiravir, fluvoxamine and Paxlovid) for COVID-19: a meta-analysis. *Ann. Med.* **54**, 516–523 (2022).

11. Lytle, C. D. & Sagripanti, J. L. Predicted inactivation of viruses of relevance to biodefense by solar radiation. *J. Virol.* **79**, 14244–14252 (2005).
12. Feng, K., Divers, E., Ma, Y. & Li, J. Inactivation of a human Norovirus surrogate, human Norovirus virus-Like particles, and vesicular stomatitis virus by gamma irradiation. *Appl. Environ. Microbiol.* **77**, 3507–3517 (2011).
13. Almeida, C. F., Purcell, D. F. J., Godfrey, D. I. & McAuley, J. L. The efficacy of common household cleaning agents for SARS-CoV-2 infection control. *Viruses* **14**, 715 (2022).
14. Ahmad Wadi, A. F. A. et al. Effects of strain differences, humidity changes, and saliva contamination on the inactivation of SARS-CoV-2 by ion irradiation. *Viruses* **16**, 520 (2024).
15. Kaczmarczyk, L. S. et al. Corona and polio viruses are sensitive to short pulses of W-band gyrotron radiation. *Environ. Chem. Lett.* **19**, 3967–3972 (2021).
16. Sun, C. K. et al. Resonant dipolar coupling of microwaves with confined acoustic vibrations in a Rod-shaped virus. *Sci. Rep.* **7**, 4611 (2017).
17. Wu, Y. & Yao, M. In situ airborne virus inactivation by microwave irradiation. *Chin. Sci. Bull.* **59**, 1438–1445 (2014).
18. Wu, Y. et al. MS2 virus inactivation by atmospheric-pressure cold plasma using different gas carriers and power levels. *Appl. Environ. Microbiol.* **81**, 996–1002 (2015).
19. Afaghi, P., Lapolla, M. A. & Ghandi, K. Denaturation of the SARS-CoV-2 Spike protein under non-thermal microwave radiation. *Sci. Rep.* **11**, 23373 (2021).
20. Hoffmann, M., Kleine-Weber, H. & Pöhlmann, S. A. Multibasic cleavage site in the Spike protein of SARS-CoV-2 is essential for infection of human lung cells. *Mol. Cell.* **78**, 779–784e5 (2020).
21. Ozono, S. et al. SARS-CoV-2 D614G Spike mutation increases entry efficiency with enhanced ACE2-binding affinity. *Nat. Commun.* **12**, 848 (2021).
22. Laporte, M. et al. The SARS-CoV-2 and other human coronavirus Spike proteins are fine-tuned towards temperature and proteases of the human airways. *PLoS Pathog.* **17**, e1009500 (2021).
23. Syed, A. M. et al. Rapid assessment of SARS-CoV-2–evolved variants using virus-like particles. *Science* **374**, 1626–1632 (2021).
24. Yang, S. C. et al. Efficient structure resonance energy transfer from microwaves to confined acoustic vibrations in viruses. *Sci. Rep.* **5**, 18030 (2015).
25. Siddharta, A. et al. Inactivation of HCV and HIV by microwave: a novel approach for prevention of virus transmission among people who inject drugs. *Sci. Rep.* **6**, 36619 (2016).
26. Arbeitman, C. R., Rojas, P., Ojeda-May, P. & Garcia, M. E. The SARS-CoV-2 Spike protein is vulnerable to moderate electric fields. *Nat. Commun.* **12**, 5407 (2021).
27. Xiao, Y. et al. Inactivation efficacy and mechanism of 9.375 ghz electromagnetic wave on coronavirus. *Virology* **598**, 110165 (2024).
28. Banting, H., Goode, I., Flores, C. E. G., Colpitts, C. C. & Saavedra, C. E. Electromagnetic deactivation spectroscopy of human coronavirus 229E. *Sci. Rep.* **13**, 8886 (2023).
29. Lipskij, A., Arbeitman, C., Rojas, P., Ojeda-May, P. & Garcia, M. E. Dramatic differences between the structural susceptibility of the S1 Pre- and S2 postfusion States of the SARS-CoV-2 Spike protein to external electric fields revealed by molecular dynamics simulations. *Viruses* **15**, 2405 (2023).
30. Anderson, M., Lopez, J., Wyr, M. & Ramirez, P. W. Defining diverse spike-receptor interactions involved in SARS-CoV-2 entry: mechanisms and therapeutic opportunities. *Virology* **607**, 110507 (2025).
31. Wang, K. et al. CD147-spike protein is a novel route for SARS-CoV-2 infection to host cells. *Sig Transduct. Target. Ther.* **5**, 283 (2020).
32. Brunetti, N. S. et al. SARS-CoV-2 uses CD4 to infect T helper lymphocytes. *Elife* **12**, e84790 (2023).
33. Clausen, T. M. et al. SARS-CoV-2 Infection Depends on Cellular Heparan Sulfate and ACE2. *Cell* 183, 1043–1057.e15 (2020).
34. Gu, Y. et al. Receptome profiling identifies KREMEN1 and ASGR1 as alternative functional receptors of SARS-CoV-2. *Cell. Res.* **32**, 24–37 (2022).
35. Thépaut, M. et al. DC/L-SIGN recognition of Spike glycoprotein promotes SARS-CoV-2 trans-infection and can be inhibited by a glycomimetic antagonist. *PLoS Pathog.* **17**, e1009576 (2021).
36. Nguyen, L. et al. Sialic acid-containing glycolipids mediate binding and viral entry of SARS-CoV-2. *Nat. Chem. Biol.* **18**, 81–90 (2022).
37. Baggen, J. et al. TMEM106B is a receptor mediating ACE2-independent SARS-CoV-2 cell entry. *Cell* **186**, 3427–3442e22 (2023).
38. Liao, Z. et al. Human transferrin receptor can mediate SARS-CoV-2 infection. *Proc. Natl. Acad. Sci. U.S.A.* 121, e2317026121 (2024).
39. Khan, I. et al. Tubeimosides are pan-coronavirus and filovirus inhibitors that can block their fusion protein binding to Niemann-Pick C1. *Nat. Commun.* **15**, 162 (2024).
40. Buonanno, M., Welch, D., Shuryak, I. & Brenner, D. J. Far-UVC light (222 nm) efficiently and safely inactivates airborne human coronaviruses. *Sci. Rep.* **10**, 10285 (2020).
41. Biasin, M. et al. UV-C irradiation is highly effective in inactivating SARS-CoV-2 replication. *Sci. Rep.* **11**, 6260 (2021).
42. Storm, N. et al. Rapid and complete inactivation of SARS-CoV-2 by ultraviolet-C irradiation. *Sci. Rep.* **10**, 22421 (2020).
43. Robinson, R. T., Mahfooz, N., Rosas-Mejia, O., Liu, Y. & Hull, N. M. UV222 disinfection of SARS-CoV-2 in solution. *Sci. Rep.* **12**, 14545 (2022).
44. Claus, H. Ozone generation by ultraviolet lamps†. *Photochem. Photobiol.* **97**, 471–476 (2021).
45. Panich, U., Sittithumcharee, G., Rathviboon, N. & Jirawatnotai, S. Ultraviolet Radiation-Induced Skin Aging: The Role of DNA Damage and Oxidative Stress in Epidermal Stem Cell Damage Mediated Skin Aging. *Stem Cells Int* 7370642 (2016). (2016).
46. Blatchley, E. R. et al. Far UV-C radiation: an emerging tool for pandemic control. *Crit. Rev. Environ. Sci. Technol.* **53**, 733–753 (2023).
47. Flatscher, J. et al. Pulsed electromagnetic fields (PEMF)-Physiological response and its potential in trauma treatment. *Int. J. Mol. Sci.* **24**, 11239 (2023).
48. Hu, H. et al. Promising application of pulsed electromagnetic fields (PEMFs) in musculoskeletal disorders. *Biomed. Pharmacother.* **131**, 110767 (2020).

Acknowledgements

We thank Dr. John Guatelli for his insightful comments on the project. This study was supported by an NSF SBIR award (#: 2035140) to Epirus, Inc. P.W.R. was supported by a New Investigator Grant (GF00610932) from the California State University Biotechnology program (CSUBIOTECH) and NIH award R16 AI184450. C.P., M.A., M.W., and J.T. were supported, in part, by awards T32GM138075, T34GM149378, TL4GM118980, UL-1GM118979, and RL5GM118978 from the National Institutes of General Medical Sciences (NIGMS).

Author contributions

Conceptualization: S.G., W.D., H.B.M., P.W.R.; Validation: C.P, F.M.A., S.G., M.A., M.W., P.W.R.; Methodology, C.P., F.M.A., M.A., M.W., S.G., J.T., A.F., P.W.R.; Project Administration: P.W.R.; Writing – Original Draft, S.G,

C.P., F.M.A., P.W.R.; Writing – Review & Editing, C.P., S.G, F.M.A., P.W.R.; Supervision, P.W.R.; Funding Acquisition: H.B.M., P.W.R.

Declarations

Competing interests
The authors declare no competing interests.

Additional information
Supplementary Information The online version contains supplementary material available at https://doi.org/10.1038/s41598-025-01896-1.

Correspondence and requests for materials should be addressed to P.W.R.

Reprints and permissions information is available at www.nature.com/reprints.

Publisher's note Springer Nature remains neutral with regard to jurisdictional claims in published maps and institutional affiliations.